Properties of Heavy Cosmic Nuclei Phosphorus, Chlorine, Argon, Potassium, and Calcium: Results from the Alpha Magnetic Spectrometer

A. Aceituno,[29] M. Aguilar,[29] B. Alpat,[35] G. Ambrosi,[35] H. Anderson,[9] J. Antunes,[21,26] L. Arruda,[26] N. Attig,[23] C. Bagwell,[9] F. Barao,[26,27] M. Barbanera,[35] L. Barrin,[13] A. Bartoloni,[39] R. Battiston,[46,47] A. Bayyari,[19] N. Belyaev,[9] B. Bertucci,[35,36] V. Bindi,[19] K. Bollweg,[20] J. Bolster,[9] M. Borchiellini,[16] B. Borgia,[39,40] M. J. Boschini,[31] M. Bourquin,[14] C. Brugnoni,[35,36] W. J. Burger,[46] H. Y. Cai,[5,6] X. D. Cai,[9] M. Capell,[9] J. Casaus,[29] J. Cassidy,[20] G. Castellini,[12] F. Cervelli,[37] Y. H. Chang,[44,45] G. M. Chen,[5,6] G. R. Chen,[22] H. Chen,[18] H. Chen,[5,6] H. S. Chen,[5,6] Y. Chen,[22] L. Cheng,[22] H. Y. Chou,[44] S. Chouridou,[1] V. Choutko,[9] C. H. Chung,[1] C. Clark,[20] G. Coignet,[3] C. Consolandi,[19] A. Contin,[7,8] C. Corti,[19] Y. X. Cui,[5,6] Z. Cui,[21,22] K. Dadzie,[9] F. D'Angelo,[7,8] A. Dass,[19] C. Delgado,[29] S. Della Torre,[31] M. B. Demirköz,[2] L. Derome,[15] S. Di Falco,[37] V. Di Felice,[41] C. Díaz,[29] F. Dimiccoli,[46,47] P. von Doetinchem,[19] F. Dong,[33] M. Dotson,[20] M. Duranti,[35] A. Egorov,[9] A. Ellison,[20] F. Faldi,[35,36] D. Fehr,[1] J. Feng,[17] E. Fiandrini,[35,36] P. Fisher,[9] V. Formato,[41] R. J. García-López,[25] A. Galdames,[9] C. Gargiulo,[13] H. Gast,[1] T. T. Ge,[17] M. Gervasi,[31,32] L. E. Ghezzer,[46,47] F. Giovacchini,[29] D. M. Gómez-Coral,[30] J. Gong,[33] D. Grandi,[31,32] M. Graziani,[35,36] R. Guidetti,[31,32] C. Guan,[21] Z. H. He,[17] B. Heber,[24] F. Hernández-Nicolás,[29] L. Höfer,[1] T. H. Hsieh,[9] J. Y. Hu,[35] B. W. Huang,[18] M. Ionica,[35] M. Incagli,[37] Yi Jia,[9] H. Jinchi,[28] T. Kappe,[1] E. Karadöller,[2] G. Karagöz,[2] J. Kastelic,[20] Th. Kirn,[1] O. Kounina,[9] A. Kounine,[9] V. Koutsenko,[9] D. Krasnopevtsev,[9] A. Kuhlman,[19] A. Kulemzin,[9] G. La Vacca,[31,32] E. Laudi,[13] G. Laurenti,[7] I. Lazzizzera,[46,47] H. T. Lee,[43] S. C. Lee,[44] H. L. Li,[22] J. H. Li,[17] J. Q. Li,[33] M. Li,[21] Q. Li,[33] Q. Li,[21] Q. Y. Li,[22] S. L. Li,[5] Z. H. Li,[5,6] P. Liao,[21] C. H. Lin,[44] T. Lippert,[23] P. C. Liu,[22] Z. Liu,[41] S. Q. Lu,[5,44] J. Z. Luo,[33] Q. Luo,[17] S. D. Luo,[18] Xi Luo,[22] C. Mañá,[29] J. Marín,[29] G. Martínez,[29] N. Masi,[7] D. Maurin,[15] T. Medvedeva,[9] A. Menchaca-Rocha,[30] Q. Meng,[33] V. V. Mikhailov,[22] M. Molero,[29] P. Mott,[20] L. Mussolin,[35,36] Y. Najafi Jozani,[1] R. Nicolaidis,[46,47] N. Nikonov,[19] F. Nozzoli,[46] J. Ocampo-Peleteiro,[7] A. Oliva,[7] M. Orcinha,[35,36] F. Palmonari,[7,8] M. Paniccia,[14] A. Pashnin,[9] M. Pauluzzi,[35,36] D. Pelosi,[35,36] S. Pensotti,[31,32] D. Perez,[9] P. Pietzcker,[24] V. Plyaskin,[9] S. Poluianov,[34] D. Pridöhl,[1] N. Puccetti,[46,47] Z. Y. Qu,[22] L. Quadrani,[7,8] M. M. Rafiei,[39] P. G. Rancoita,[31] D. Rapin,[14] E. Robyn,[7] I. Rodríguez-García,[29] L. Romaneehsen,[24] F. Rossi,[46,47] A. Rozhkov,[9] D. Rozza,[31,32] R. Sagdeev,[10] S. Schael,[1] A. Schultz von Dratzig,[1] G. Schwering,[1] E. S. Seo,[11] B. S. Shan,[4] A. Shukla,[19] T. Siedenburg,[1] A. Siemko,[9] G. Silvestre,[35] D. Schledewitz,[46,47] J. W. Song,[21] X. J. Song,[22] R. Sonnabend,[1] A. Strekalovsky,[9] L. Strigari,[39,*] A. Stuzhin,[21] T. Su,[22] Q. Sun,[21] Z. T. Sun,[5] L. Tabarroni,[41] M. Tacconi,[31,32] Z. C. Tang,[5] J. J. Teoh,[5,6] J. Tian,[41] Ye Tian,[5,6] Y. Tian,[18] Samuel C. C. Ting,[9,13] S. M. Ting,[9] N. Tomassetti,[35,36] J. Torsti,[48] A. Ubaldi,[35,36] I. Usoskin,[34] V. Vagelli,[38,35] R. Vainio,[48] P. Väisänen,[34] M. Valencia-Otero,[44] E. Valente,[39,40] E. Valtonen,[48] E. Van Hove,[9] M. Vázquez Acosta,[25] M. Vecchi,[16] M. Velasco,[29] J. C. Wang,[5] L. Q. Wang,[21] N. H. Wang,[21] S. Wang,[19] X. Wang,[9] Z. M. Wang,[22] M. Waqas,[41] Z. L. Weng,[9] H. Wu,[33] Z. B. Wu,[21] J. N. Xiao,[18] R. Q. Xiong,[33] Y. Z. Xiong,[18] W. Xu,[21,22] Q. Yan,[5,6] Z. X. Yan,[5,6] H. T. Yang,[5,6] Y. Yang,[42,44] H. Yi,[33] Y. H. You,[5,6] M. Yu,[21] Y. M. Yu,[9] Z. Q. Yu,[5] B. Q. Yuan,[22] C. Zhang,[5] F. Z. Zhang,[5] J. Zhang,[21] J. H. Zhang,[33] Z. Zhang,[9] P. W. Zhao,[17] Z. M. Zheng,[4] H. F. Zhou,[17] H. L. Zhuang,[5] V. Zhukov,[1] L. K. Zou,[22] M. Zuberi,[9] and P. Zuccon[46,47]

(AMS Collaboration)

[1]*I. Physics Institute and JARA-FAME, RWTH Aachen University, 52056 Aachen, Germany*
[2]*Department of Physics, Middle East Technical University (METU), 06800 Ankara, Türkiye*
[3]*Université Grenoble Alpes, Université Savoie Mont Blanc, CNRS, LAPP-IN2P3, 74000 Annecy, France*
[4]*Beihang University (BUAA), Beijing, 100191, China*
[5]*Institute of High Energy Physics (IHEP), Chinese Academy of Sciences, Beijing, 100049, China*
[6]*University of Chinese Academy of Sciences (UCAS), Beijing, 100049, China*
[7]*INFN Sezione di Bologna, 40126 Bologna, Italy*
[8]*Università di Bologna, 40126 Bologna, Italy*
[9]*Massachusetts Institute of Technology (MIT), Cambridge, Massachusetts 02139, USA*
[10]*East-West Center for Space Science, University of Maryland, College Park, Maryland 20742, USA*
[11]*IPST, University of Maryland, College Park, Maryland 20742, USA*
[12]*CNR–IROE, 50125 Firenze, Italy*
[13]*European Organization for Nuclear Research (CERN), 1211 Geneva 23, Switzerland*
[14]*DPNC, Université de Genève, 1211 Genève 4, Switzerland*
[15]*Université Grenoble Alpes, CNRS, Grenoble INP, LPSC-IN2P3, 38000 Grenoble, France*

[16]*Kapteyn Astronomical Institute, University of Groningen, P.O. Box 800, 9700 AV Groningen, Netherlands*
[17]*Sun Yat–sen University (SYSU), Guangzhou, 510275, China*
[18]*Zhejiang University (ZJU), Hangzhou 310058, China*
[19]*Physics and Astronomy Department, University of Hawaii, Honolulu, Hawaii 96822, USA*
[20]*National Aeronautics and Space Administration Johnson Space Center (JSC), Houston, Texas 77058, USA and Goddard Space Flight Center (GSFC), Greenbelt, Maryland 20771, USA*
[21]*Shandong University (SDU), Jinan, Shandong, 250100, China*
[22]*Shandong Institute of Advanced Technology (SDIAT), Jinan, Shandong, 250100, China*
[23]*Jülich Supercomputing Centre and JARA-FAME, Research Centre Jülich, 52425 Jülich, Germany*
[24]*Institut für Experimentelle und Angewandte Physik, Christian-Albrechts-Universität zu Kiel, 24118 Kiel, Germany*
[25]*Instituto de Astrofísica de Canarias (IAC), 38205 La Laguna, Santa Cruz de Tenerife, Spain and Departamento de Astrofísica, Universidad de La Laguna, 38206 La Laguna, Tenerife, Spain*
[26]*Laboratório de Instrumentação e Física Experimental de Partículas (LIP), 1649-003 Lisboa, Portugal*
[27]*Departamento de Física, Instituto Superior Técnico (IST), Universidade de Lisboa, 1049-001 Lisboa, Portugal*
[28]*National Chung–Shan Institute of Science and Technology (NCSIST), Longtan, Tao Yuan, 32546, Taiwan*
[29]*Centro de Investigaciones Energéticas, Medioambientales y Tecnológicas (CIEMAT), 28040 Madrid, Spain*
[30]*Instituto de Física, Universidad Nacional Autónoma de México (UNAM), Ciudad de México, 01000 Mexico*
[31]*INFN Sezione di Milano–Bicocca, 20126 Milano, Italy*
[32]*Università di Milano–Bicocca, 20126 Milano, Italy*
[33]*Southeast University (SEU), Nanjing, 210096, China*
[34]*Sodankylä Geophysical Observatory and Space Physics and Astronomy Research Unit, University of Oulu, 90014 Oulu, Finland*
[35]*INFN Sezione di Perugia, 06100 Perugia, Italy*
[36]*Università di Perugia, 06100 Perugia, Italy*
[37]*INFN Sezione di Pisa, 56100 Pisa, Italy*
[38]*Agenzia Spaziale Italiana (ASI), 00133 Roma, Italy*
[39]*INFN Sezione di Roma 1, 00185 Roma, Italy*
[40]*Università di Roma La Sapienza, 00185 Roma, Italy*
[41]*INFN Sezione di Roma Tor Vergata, 00133 Roma, Italy*
[42]*National Cheng Kung University, Tainan, 70101, Taiwan*
[43]*Academia Sinica Grid Center (ASGC), Nankang, Taipei, 11529, Taiwan*
[44]*Institute of Physics, Academia Sinica, Nankang, Taipei, 11529, Taiwan*
[45]*Physics Department and Center for High Energy and High Field Physics, National Central University (NCU), Tao Yuan, 32054, Taiwan*
[46]*INFN TIFPA, 38123 Trento, Italy*
[47]*Università di Trento, 38123 Trento, Italy*
[48]*Space Research Laboratory, Department of Physics and Astronomy, University of Turku, 20014 Turku, Finland*

(Received 23 February 2026; accepted 30 April 2026; published 17 June 2026)

We report the unique properties of cosmic phosphorus (P), chlorine (Cl), argon (Ar), potassium (K), and calcium (Ca) fluxes in the GV to TV rigidity range collected by the Alpha Magnetic Spectrometer (AMS) on the International Space Station. With a total of one million events collected over 13.5 years, we observed that the rigidity dependencies of the five fluxes are well described by the sums of a primary cosmic ray component and a secondary cosmic ray component. The abundance ratios of all five elements to Si at the source are accurately determined independent of cosmic ray propagation. The source abundance of Ar and Ca (even-Z elements) is larger than P, Cl, and K (odd-Z elements). The secondary components of the P and the Cl fluxes are each $\sim 1/3$ of the F flux, and the secondary components of the Ar, K, and Ca fluxes are each $\sim 1/2$ of the F flux. The twenty elements measured by AMS, from He to Ca and Fe, can be categorized into four classes, two primary and two secondary, based on their rigidity dependence.

DOI: 10.1103/d2vf-fw3v

Introduction—Heavy cosmic rays phosphorus (P), chlorine (Cl), potassium (K), argon (Ar), and calcium (Ca) are thought to be produced both in astrophysical sources and by the collisions of heavier nuclei with the interstellar medium [1]. Little is known about their properties.

Previously, measurements of the cosmic Na and Al fluxes with the Alpha Magnetic Spectrometer (AMS) have

---

[*] Also at IRCCS Azienda Ospedaliero-Universitaria di Bologna, Bologna, Italy.

been reported [2]. Remarkably, the Na and Al fluxes were found to be well described by the sum of a primary component (proportional to the Si flux [3]) and a secondary component (proportional to the F flux [4]). Recently, AMS reported that dominantly primary Ne, Mg, and S fluxes are also well described over the entire rigidity range by the sum of a primary component (proportional to the Si flux) and a secondary component (proportional to the F flux). In particular, it was found that the primary and secondary contributions of the even-Z element fluxes of Ne, Mg, and S are distinctly different from the primary and secondary contributions of the odd-Z element Na and Al fluxes [5].

Over the past 50 years, a few cosmic ray experiments have measured the P, Cl, Ar, K, and Ca fluxes in kinetic energy [6–14]. The measurement errors exceed 50% at ~50 GeV/n (~100 GV in rigidity). There are no measurements of these fluxes in rigidity. Precise knowledge of the rigidity dependence of the P, Cl, Ar, K, and Ca fluxes will provide important insights on cosmic ray production, acceleration, and propagation.

In this Letter we report the precise measurement of the P, Cl, and K fluxes in cosmic rays in the rigidity range from 2.15 GV to 1.2 TV and the Ar and Ca fluxes in cosmic rays in the rigidity range from 2.15 GV to 3.0 TV based on a total of $\sim 10^6$ (P, Cl, K, Ar, and Ca) nuclei collected by AMS during the first 13.5 years (May 19, 2011 to November 26, 2024) of operation aboard the International Space Station. The total flux errors at 100 GV are ~6% for Ar and Ca and ~8% for P, Cl, and K.

Detector—The layout and description of the AMS detector are presented in Refs. [15,16] and shown in Fig. S1 of the Supplemental Material [17]. The key elements used in this measurement are the permanent magnet [20]; the nine layers, $L1$–$L9$, of the silicon tracker [21–24]; and the four planes of the time of flight (TOF) scintillation counters [25]. Further information on the AMS layout, performance, trigger, and the Monte Carlo simulations (MC) [26–28] is included in the Supplemental Material [17].

Event selection—In the first 13.5 years, AMS has collected 2.4×10^{11} cosmic ray events. Cosmic ray nuclei are required to be downward going and to have a reconstructed track in the inner tracker; see Fig. S3 of the Supplemental Material [17] for a reconstructed P event. Details of the event selection are contained in the Supplemental Material [17] and in Refs. [26,29].

With this selection, the charge confusion from noninteracted nuclei due to the finite AMS charge resolution is $< 2\%$ for P and $< 1\%$ for Cl, Ar, K, and Ca over the entire rigidity range; see Fig. S4 of the Supplemental Material [17]. The main sources of background come from interactions of heavier nuclei, such as S, Cl, Ar, K, Ca, Sc, Ti, V, Cr, and Fe, in the AMS materials above tracker $L2$. The background resulting from interactions in the material between $L1$ and $L2$ (Transition Radiation Detector and upper TOF) is evaluated by fitting the charge distribution of tracker $L1$ with charge distribution templates of Si to Ti, as shown in Fig. S5 of the Supplemental Material [17]. The charge distribution templates are obtained at $L2$ from a selection of noninteracting samples of Si to Ti by requiring that $L1$, upper TOF, and $L3$–$L8$ measure the same charge value. After the cut on the $L1$ charge, the residual background varies from 2% to 20% depending on rigidity and the nuclei. The background from interactions on materials above $L1$ (thin support structures made by carbon fiber and aluminum honeycomb) has been estimated from simulation using MC samples generated according to AMS flux measurements [17,30,31]. The simulation of nuclear interactions has been validated with data using nuclear charge changing cross sections (e.g., S, Ar, Ca, $\mathrm{Fe} \rightarrow \mathrm{P} + X$) measured by AMS [28]. For P, this background is estimated to be 10% at 2.15 GV, 14% at 10 GV, 13% at 100 GV, and 10% at 1.2 TV, and $< 8\%$ for other nuclei over the entire rigidity range.

We obtain 0.17×10^6 P, 0.14×10^6 Cl, 0.17×10^6 K, 0.21×10^6 Ar, and 0.30×10^6 Ca nuclei after background subtraction.

Data analysis—The isotropic flux Φ_i in the ith rigidity bin $(R_i, R_i + \Delta R_i)$ is given by

$$\Phi_i = \frac{N_i}{A_i \epsilon_i T_i \Delta R_i}, \tag{1}$$

where N_i is the number of events corrected for bin-to-bin migration, A_i is the effective acceptance including geometric acceptance, event reconstruction and selection efficiencies, and inelastic interactions of nuclei in the AMS materials, ϵ_i is the trigger efficiency, and T_i is the collection time. In this Letter P, Cl, and K fluxes were measured in 46 bins from 2.15 GV to 1.2 TV, and Ar and Ca fluxes were measured in 47 bins from 2.15 GV to 3.0 TV with bin widths chosen according to the rigidity resolution and available statistics. The resulting bin widths are identical with our previous publication on the S flux [5].

The bin-to-bin migration of events was corrected using the unfolding procedure described in Ref. [29]. These corrections, $(N_i - \aleph_i)/\aleph_i$ where $\aleph_i$ is the number of observed events in bin i, are $+25\%$ at 3 GV changing smoothly to $+8\%$ at 10 GV, -2% at 100 GV, -10% at 300 GV, and -21% at 1.2 TV for P flux and similar for the Cl and K fluxes. For the Ca flux these corrections are $+30\%$ at 3 GV changing smoothly to $+10\%$ at 10 GV, -1% at 100 GV, -5% at 300 GV, -16% at 1.2 TV, and -5% at 3.0 TV, and similar for the Ar flux.

Extensive studies were made of the systematic errors. These errors include the uncertainties in the background evaluation discussed above, the trigger efficiency, the geomagnetic cutoff factor [17], the acceptance calculation, the rigidity resolution function, and the absolute rigidity scale.

The systematic flux errors due to background subtraction are $< 5\%$ for the P flux and $< 3\%$ for the Cl, K, Ar, and Ca fluxes over the entire rigidity range.

The systematic error on the flux associated with the trigger efficiency measurement is $<1\%$ over the entire rigidity range.

The geomagnetic cutoff factor was varied from 1.0 to 1.4, resulting in a negligible systematic uncertainty ($< 0.1\%$) in the rigidity range below 30 GV.

The effective acceptances A_i were calculated using MC simulation and corrected for small differences between the data and simulated events related to (a) event reconstruction and selection, namely in the efficiencies of velocity vector determination, track finding, charge determination, and tracker quality cuts and (b) the details of inelastic interactions of nuclei in the AMS materials; see the discussion in the Supplemental Material [17]. The total corrections to the effective acceptances from the differences between data and MC simulation were found to be $< 5\%$ over the entire rigidity range for all fluxes. The systematic error on the flux associated with the reconstruction and selection is $< 2\%$ over the entire rigidity range. The survival probabilities of different nuclei due to interactions in the AMS materials were evaluated using inelastic cross sections measured by AMS as described in Ref. [28]. The uncertainty in the inelastic cross sections is $< 4\%$ up to 100 GV. Above 100 GV, the small rigidity dependence of the cross sections from the Glauber-Gribov model [27] was treated as an uncertainty and added in quadrature to the uncertainties from the measured inelastic cross sections. The corresponding systematic errors on the fluxes are $< 4\%$ up to 100 GV and rise smoothly to 5% at 3.0 TV.

The rigidity resolution functions have pronounced Gaussian cores characterized by widths σ and non-Gaussian tails more than 2.5σ away from the center [26]. The systematic error on the fluxes due to the rigidity resolution function was obtained by repeating the unfolding procedure while varying the width of the Gaussian core of the resolution function by 5% and by independently varying the amplitudes of the non-Gaussian tails by 10% [26]. The resulting systematic error on the fluxes is 4% at 2 GV, $< 1\%$ from 3 to 300 GV, and increases smoothly to 3% at 1.2 TV and 6% at 3 TV.

There are two contributions to the systematic uncertainty on the rigidity scale [24,29]. The first is due to time dependent residual tracker misalignment. This error was estimated by comparing the E/p ratio for electrons and positrons, where E is the energy measured with the electromagnetic calorimeter and p is the momentum measured with the tracker. This error was found to be $1/34\ \mathrm{TV}^{-1}$ [24]. The second systematic error on the rigidity scale arises from the magnetic field map measurement and its temperature corrections [29]. The overall error on the fluxes due to uncertainty on the rigidity scale is $< 1\%$ up to 300 GV and increases smoothly to 2% at 1.2 TV and to 6% at 3 TV.

Most importantly, several independent analyses were performed on the same data sample by different study groups. The results of those analyses are consistent with this Letter.

Results—The measured P, Cl, Ar, K, and Ca fluxes, Φ_{P}, Φ_{Cl}, Φ_{Ar}, Φ_{K}, Φ_{Ca}, including statistical and systematic errors are reported in Tables SI–SV of the Supplemental Material [17,32] as a function of the rigidity at the top of the AMS detector. Figure 1 shows the AMS P, Cl, K, Ar,

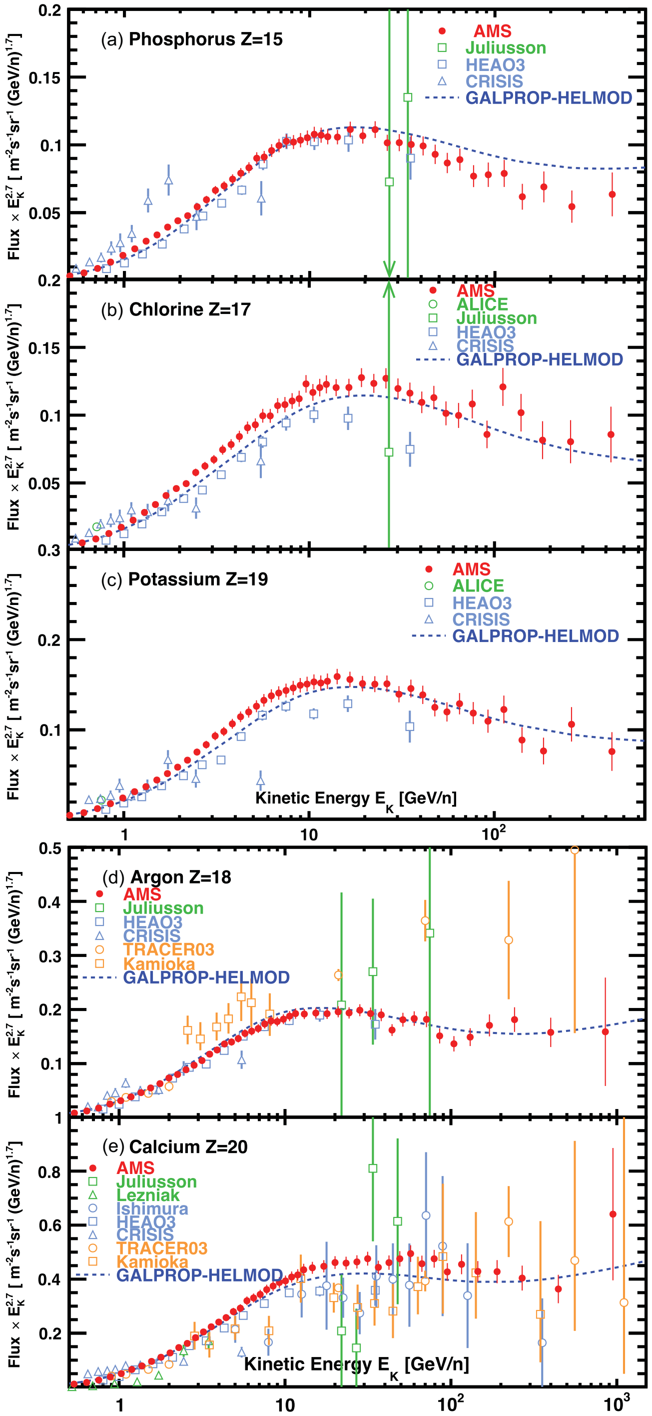

FIG. 1. The AMS (a) P, (b) Cl, (c) K, (d) Ar, and (e) Ca fluxes as a function of kinetic energy per nucleon E_K multiplied by $E_K^{2.7}$ together with other measurements [6–13] and with the predictions of the most recent cosmic ray model GALPROP–HELMOD [33]. See also Fig. S8 of the Supplemental Material [17].

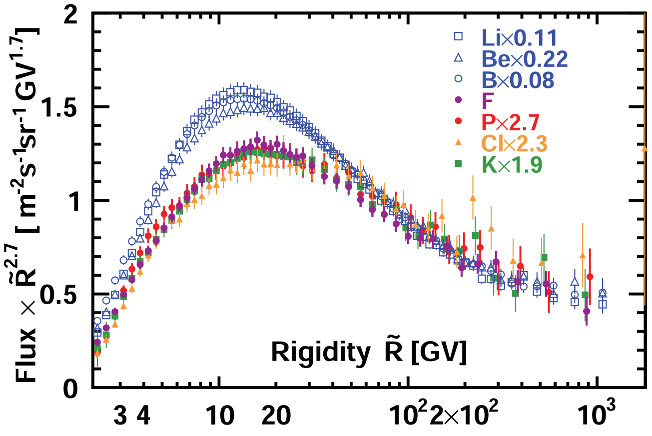

FIG. 2. The AMS P, Cl, and K fluxes with total errors as a function of rigidity $\tilde{R}$ together with the AMS F flux and with the AMS Li, Be, and B fluxes. As seen, the rigidity dependence of P, Cl, K, and F fluxes are very similar and different from the Li, Be, and B flux rigidity dependence. For display purposes only, the Li, Be, B, P, Cl, and K fluxes were scaled as indicated.

and Ca fluxes as a function of kinetic energy per nucleon together with the previous measurements and with the predictions of the most recent cosmic ray model GALPROP–HELMOD, which uses the AMS data [33]. As seen, AMS results are distinct from other measurements both in accuracy and energy range. To compare the rigidity dependence of the five fluxes with the heavy primary cosmic ray Si flux Φ_{Si} and the secondary cosmic ray F flux Φ_{F}, the measurements of the Si and F fluxes [3,4] were extended to the 13.5 year period and rebinned. They are reported in Tables SVI and SVII of the Supplemental Material [17,32]. We have also extended to the 13.5 year period the S flux Φ_{S} [5]. It is reported in Table SVIII of the Supplemental Material [17,32]. The odd-Z to even-Z flux ratios $\Phi_{\mathrm{P}}/\Phi_{\mathrm{S}}$, $\Phi_{\mathrm{Cl}}/\Phi_{\mathrm{Ar}}$, and $\Phi_{\mathrm{K}}/\Phi_{\mathrm{Ca}}$ are reported in Tables SIX–SXI and shown in Fig. S9 of the Supplemental Material [17,32] together with the predictions of the GALPROP–HELMOD model [33]. As seen, the GALPROP–HELMOD model does not describe the AMS results.

P, Cl, and K are expected to be mostly secondary cosmic rays. Figure 2 shows AMS P, Cl, and K fluxes together with the AMS secondary F flux and the AMS secondary Li, Be, and B fluxes [34] as a function of rigidity $\tilde{R}$ with the total errors. In this and the subsequent figures, the points are placed along the abscissa at $\tilde{R}$ calculated for a flux $\propto R^{-2.7}$ [35]. As seen, the rigidity dependence of P, Cl, K, and F fluxes is very similar and different from the Li, Be, and B fluxes' rigidity dependence.

To study the small differences between Φ_{P}, Φ_{Cl}, Φ_{K}, and Φ_{F} rigidity dependencies in detail, fits of $\Phi_{\mathrm{P}}/\Phi_{\mathrm{F}}$, $\Phi_{\mathrm{Cl}}/\Phi_{\mathrm{F}}$, and $\Phi_{\mathrm{K}}/\Phi_{\mathrm{F}}$ were performed above ~3–4 GV with

$$\frac{\Phi_X}{\Phi_{\mathrm{F}}} = \begin{cases} k^X (R/R_0^X)^{\Delta_1^X}, & R \le R_0^X \text{ GV}, \\ k^X (R/R_0^X)^{\Delta_2^X}, & R > R_0^X \text{ GV}, \end{cases} \tag{2}$$

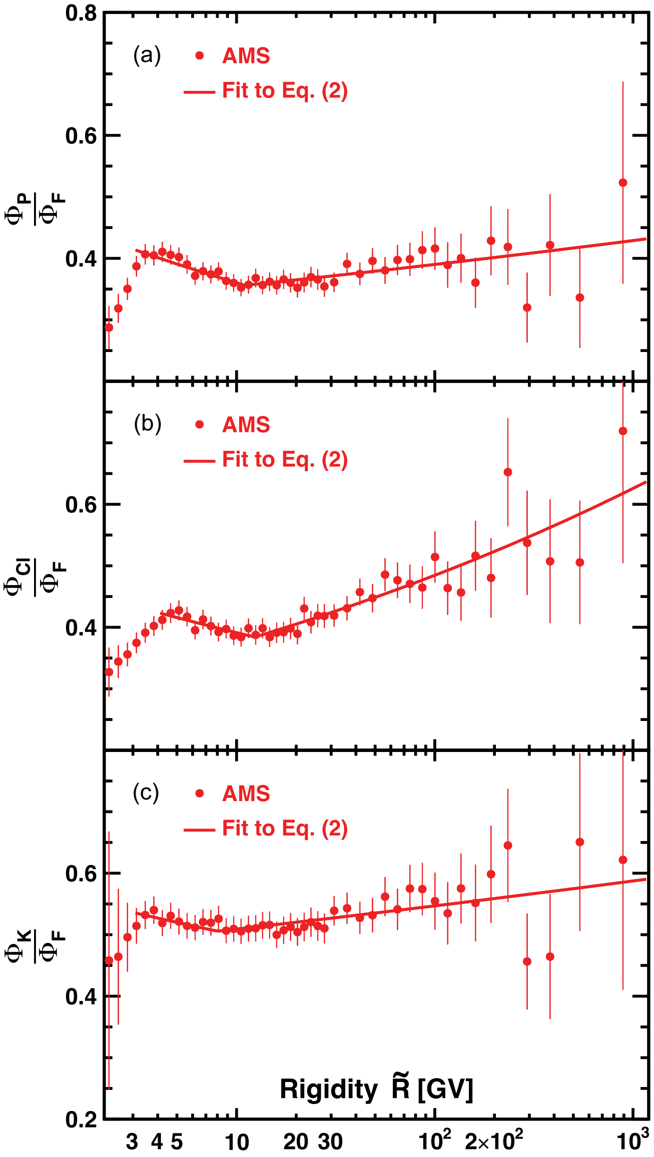

FIG. 3. The rigidity dependence of the (a) $\Phi_{\mathrm{P}}/\Phi_{\mathrm{F}}$, (b) $\Phi_{\mathrm{Cl}}/\Phi_{\mathrm{F}}$, and (c) $\Phi_{\mathrm{K}}/\Phi_{\mathrm{F}}$ together with the Eq. (2) fit results.

where k^X, R_0^X, Δ_1^X, Δ_2^X are fit parameters and $X = \mathrm{P}$, Cl, or K. The fit results are summarized in Table SXII of the Supplemental Material [17] and shown in Fig. 3.

The differences in the Φ_{P}, Φ_{Cl}, Φ_{K}, and Φ_{F} rigidity dependencies at high rigidities ($\Delta_2 \neq 0$) could be due to the presence of primary components $\propto \Phi_{\mathrm{Si}}$, $p^{\mathrm{P}}\Phi_{\mathrm{Si}}$, $p^{\mathrm{Cl}}\Phi_{\mathrm{Si}}$, and $p^{\mathrm{K}}\Phi_{\mathrm{Si}}$, in the Φ_{P}, Φ_{Cl}, and Φ_{K} respectively. To study this we have fit $\Phi_{\mathrm{P}}/\Phi_{\mathrm{F}}$, $\Phi_{\mathrm{Cl}}/\Phi_{\mathrm{F}}$, and $\Phi_{\mathrm{K}}/\Phi_{\mathrm{F}}$ with

$$\frac{\Phi_X}{\Phi_{\mathrm{F}}} = p^X \frac{\Phi_{\mathrm{Si}}}{\Phi_{\mathrm{F}}} + \begin{cases} k^X (R/R_0^X)^{\Delta_1^X}, & R \le R_0^X \text{ GV}, \\ k^X, & R > R_0^X \text{ GV}, \end{cases} \tag{3}$$

where p^X, k^X, R_0^X, Δ_1^X are fit parameters and $X = \mathrm{P}$, Cl, or K. Figure S10 of the Supplemental Material [17] shows the corresponding fit results. We conclude that the presence of

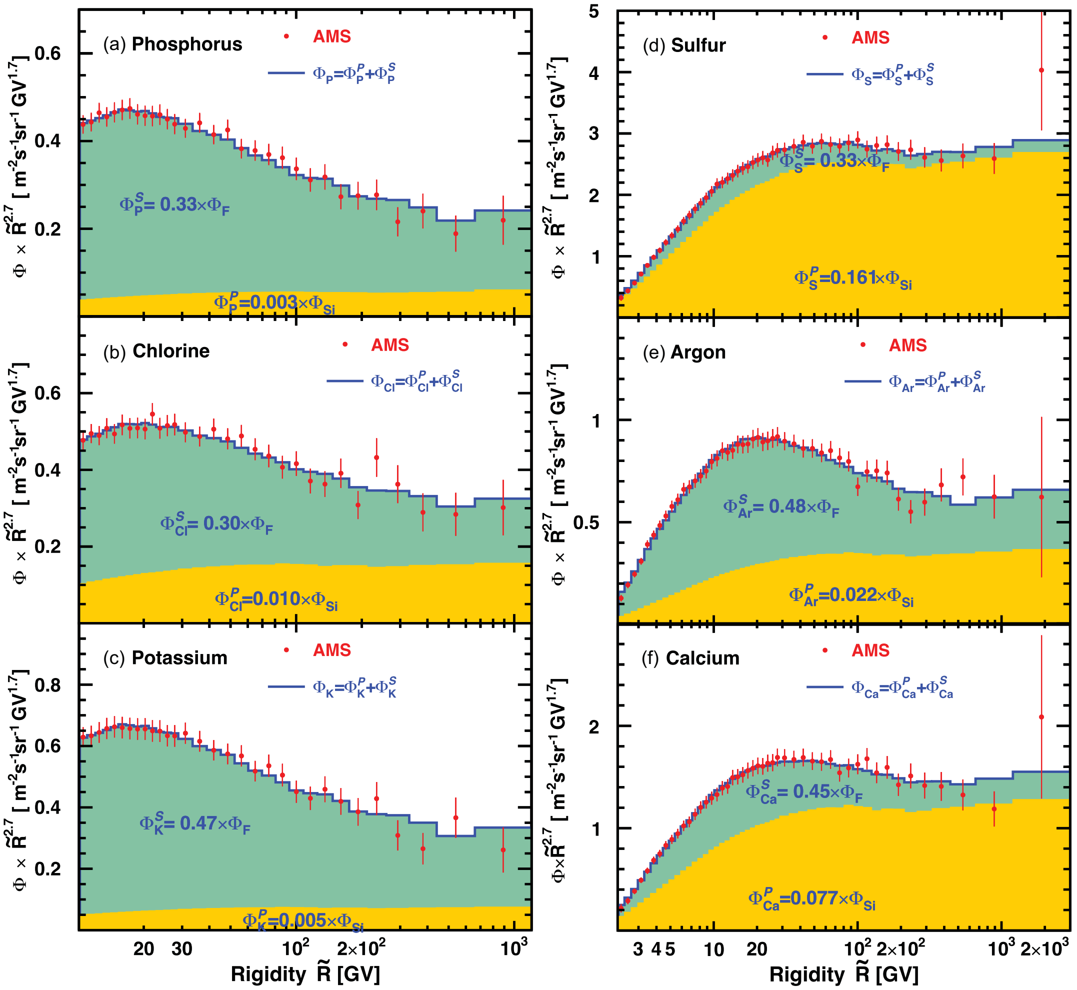

FIG. 4. The AMS (a) P, (b) Cl, (c) K, (d) S, (e) Ar, and (f) Ca fluxes fit to the weighted sum of Si and F fluxes above 10 GV for (a)–(c) and above 2.15 GV for (d)–(f). The contributions of the primary and secondary components are indicated by the shading (yellow and green, respectively). See also Table I.

a primary component which amounts to a few per mill of the Si flux can explain the small differences in the P, Cl, and K fluxes and F flux rigidity dependence at high rigidities and that consequently the P, Cl, K, and F fluxes belong to the same class of dominantly secondary cosmic rays. We also conclude that above ~10 GV, Φ_{P}, Φ_{Cl}, and Φ_{K} could be presented as the sum of a primary component (proportional to Φ_{Si}) and a secondary component (proportional to Φ_{F}). Similarly, we fit $\Phi_{\mathrm{Ar}}/\ \Phi_{\mathrm{F}}$ and $\Phi_{\mathrm{Ca}}/\ \Phi_{\mathrm{F}}$ with Eq. (3) for $X = \mathrm{Ar}$ and Ca respectively, above 2.15 GV and above

TABLE I. The primary and secondary components of P ($Z = 15$), S ($Z = 16$), Cl ($Z = 17$), Ar ($Z = 18$), K ($Z = 19$), and Ca ($Z = 20$) fluxes, their primary fractions at 10 GV, 100 GV, and 1 TV; and the χ^2/d.o.f. values of the flux fits with a linear combination of primary and secondary components for P, S, Cl, Ar, K, and Ca fluxes.

			Primary fraction, %			
Nuclei flux	Primary	Secondary	10 GV	100 GV	1 TV	χ^2/d.o.f.
Φ_{P}	$(0.0034 \pm 0.0014) \times \Phi_{\mathrm{Si}}$	$(0.33 \pm 0.01) \times \Phi_{\mathrm{F}}$	8 ± 3	17 ± 5	24 ± 7	9/29
Φ_{S}	$(0.161 \pm 0.005) \times \Phi_{\mathrm{Si}}$	$(0.33 \pm 0.04) \times \Phi_{\mathrm{F}}$	81 ± 2	90 ± 1	93 ± 1	11/46
Φ_{Cl}	$(0.0097 \pm 0.0015) \times \Phi_{\mathrm{Si}}$	$(0.30 \pm 0.02) \times \Phi_{\mathrm{F}}$	21 ± 3	38 ± 5	43 ± 7	12/29
Φ_{Ar}	$(0.022 \pm 0.002) \times \Phi_{\mathrm{Si}}$	$(0.48 \pm 0.02) \times \Phi_{\mathrm{F}}$	28 ± 2	47 ± 3	57 ± 3	24/46
Φ_{K}	$(0.0046 \pm 0.0016) \times \Phi_{\mathrm{Si}}$	$(0.47 \pm 0.02) \times \Phi_{\mathrm{F}}$	8 ± 3	16 ± 5	22 ± 7	10/29
Φ_{Ca}	$(0.077 \pm 0.003) \times \Phi_{\mathrm{Si}}$	$(0.45 \pm 0.03) \times \Phi_{\mathrm{F}}$	59 ± 2	77 ± 2	83 ± 2	13/46

4 GV. The fit results above 2.15 GV are shown in Fig. S11 of the Supplemental Material [17]. As seen, over the entire rigidity range the Φ_{Ar} and Φ_{Ca} could be presented as the sum of a primary component (proportional to Φ_{Si}) and a secondary component (proportional to Φ_{F}). Table SXIII of the Supplemental Material [17] summarizes all results of fitting Eq. (3) for the five flux ratios.

Following Refs. [2,5] to obtain the primary Φ^P_{P}, Φ^P_{S}, Φ^P_{Cl}, Φ^P_{Ar}, Φ^P_{K}, Φ^P_{Ca}, and secondary Φ^S_{P}, Φ^S_{S}, Φ^S_{Cl}, Φ^S_{Ar}, Φ^S_{K}, Φ^S_{Ca} components of the P, S, Cl, K, Ar, and Ca fluxes, we fit a linear combination of $\Phi^P \propto \Phi_{\mathrm{Si}}$ and $\Phi^S \propto \Phi_{\mathrm{F}}$ to each of these fluxes, i.e., $\Phi_{\mathrm{P}} = \Phi^P_{\mathrm{P}} + \Phi^S_{\mathrm{P}}$, $\Phi_{\mathrm{Cl}} = \Phi^P_{\mathrm{Cl}} + \Phi^S_{\mathrm{Cl}}$, $\Phi_{\mathrm{K}} = \Phi^P_{\mathrm{K}} + \Phi^S_{\mathrm{K}}$, $\Phi_{\mathrm{S}} = \Phi^P_{\mathrm{S}} + \Phi^S_{\mathrm{S}}$, $\Phi_{\mathrm{Ar}} = \Phi^P_{\mathrm{Ar}} + \Phi^S_{\mathrm{Ar}}$, and $\Phi_{\mathrm{Ca}} = \Phi^P_{\mathrm{Ca}} + \Phi^S_{\mathrm{Ca}}$. The fit is performed above 10 GV for the Φ_{P}, Φ_{Cl}, and Φ_{K}, and above 2.15 GV for the Φ_{S}, Φ_{Ar}, and Φ_{Ca}. Figure 4 shows the corresponding fit results. Table I summarizes the primary and secondary components of the P, S, Cl, Ar, K, and Ca fluxes together with the primary fractions at different rigidities. As seen, the primary components of the S, Ar, and Ca fluxes (even-Z) are larger than the primary components of the P, Cl, and K fluxes (odd-Z). The secondary components of the P, S, and Cl fluxes are each $\sim 1/3$ of the Φ_{F}, and the secondary components of the Ar, K, and Ca fluxes are each $\sim 1/2$ of the Φ_{F}. To study the stability of the determination of the primary and secondary components for Ar and Ca we have changed the fit lowest rigidity value from 2.15 GV to 10 GV, similar to the P, Cl, and K fluxes. The resulting values for the primary and secondary components for Ar and Ca with different fitting ranges agree with each other.

The observation that the cosmic ray fluxes of P, Cl, Ar, K, and Ca are the linear combinations of primary and secondary fluxes permits the direct determination of the P/Si, Cl/Si, Ar/Si, K/Si, and Ca/Si abundance ratios at the source without the need to consider models of the Galactic propagation of cosmic rays [2]. Table SXIV of the Supplemental Material [17] shows AMS model independent results on the cosmic nuclei flux ratios at the source over a wide energy range together with model-dependent results from low-energy measurements [6,36–39]. The AMS results for Ar, K, and Ca agree with most of the previous results within their measurement errors. AMS results for P, S, and Cl differ from some previous results. Figure 5(a) presents cosmic nuclei fluxes measured by AMS as a function of rigidity above 30 GV for $Z = 2$ to $Z = 20$ and $Z = 26$, [2,3,17,30,34,40]. It shows that there are two classes of dominantly primary cosmic rays, He-C-O-Fe (Primary I) and Ne-Mg-Si-S (Primary II), and two classes of secondary cosmic rays, Li-Be-B (Secondary I) and F-P-K (Secondary II). Other elements are combinations of primary and secondary cosmic rays; see Fig. S12 and Table SXV of the Supplemental Material [17] for the details. As shown in Fig. 5(b), the twenty elements from He to Ca and Fe measured by AMS can be categorized into four classes based on their rigidity dependence.

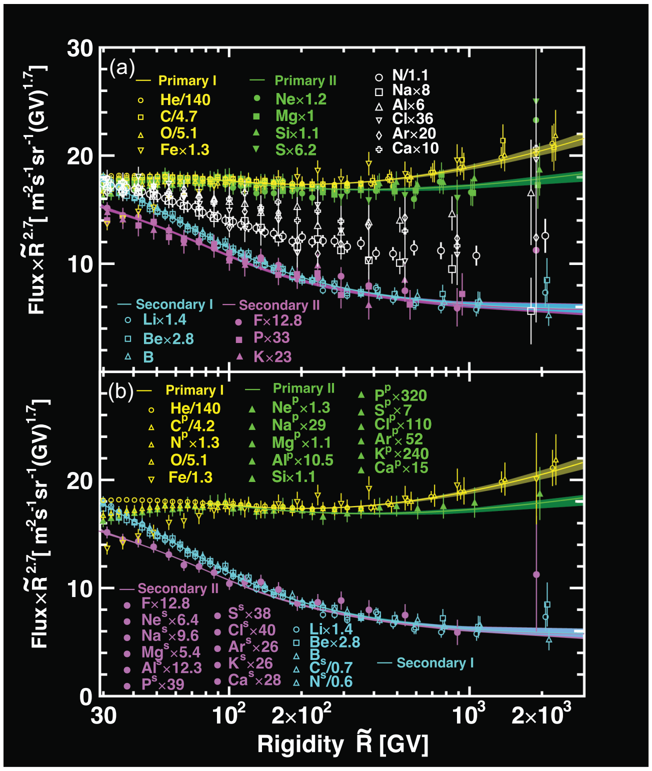

FIG. 5. (a) The twenty fluxes of cosmic-ray nuclei from He to Ca and Fe measured by AMS as a function of rigidity above 30 GV [2,3,17,30,34,40]. As seen, there are two classes of dominantly primary cosmic rays, He-C-O-Fe (Primary I) and Ne-Mg-Si-S (Primary II), and two classes of secondary cosmic rays, Li-Be-B (Secondary I) and F-P-K (Secondary II). Elements N, Na, Al, Cl, Ar, and Ca are combinations of primary and secondary cosmic rays; see Figs. 4 and S12 of the Supplemental Material [17]. (b) The fluxes of cosmic nuclei measured by AMS as functions of rigidity above 30 GV, shown as the decomposition of their primary and secondary components. For both (a) and (b): the shaded areas show the combined fit result with Eq. (5) from Ref. [3] of the Primary I fluxes (yellow), the Primary II fluxes (green), the Secondary I fluxes (cyan), and the Secondary II fluxes (magenta) together with fit errors. As seen, the twenty elements from He to Ca and Fe can be categorized into four classes based on their rigidity dependence.

In conclusion, we have presented precision measurements of the P, Cl, and K fluxes from 2.15 GV to 1.2 TV and Ar and Ca fluxes from 2.15 GV to 3.0 TV with detailed studies of the systematic errors. We found that, similar to Ne, Na, Mg, and Al, the rigidity dependencies of the P, Cl, Ar, K, and Ca fluxes are well described by the sums of a primary cosmic ray component and a secondary cosmic ray component. The primary components of the even-Z element fluxes of Ar and Ca are larger than primary components of the odd-Z element P, Cl, and K fluxes. The secondary components of the P and the Cl fluxes are each $\sim 1/3$ of the F flux, and the secondary components of the Ar, K, and Ca fluxes are each $\sim 1/2$ of the F flux. The abundance ratio at the source for P/Si is 0.0034 ± 0.0014, for Cl/Si is 0.0097 ± 0.0015, for Ar/Si is 0.022 ± 0.002, for K/Si is 0.0046 ± 0.0016, and for Ca/Si is 0.077 ± 0.003. These values are determined independent of cosmic ray propagation. We found that there are two classes of dominantly primary cosmic rays, He-C-O-Fe (Primary I) and Ne-Mg-Si-S (Primary II), and two classes of secondary cosmic rays, Li-Be-B (Secondary I) and F-P-K (Secondary II). Other elements are combinations of primary and secondary cosmic rays. The twenty elements from He to Ca and Fe measured by AMS can be categorized into four classes based on their rigidity dependence.

Acknowledgments—We are grateful for important physics discussions with Igor Moskalenko and Subir Sarkar. We thank former NASA Administrator Daniel S. Goldin for his dedication to the legacy of the ISS as a scientific laboratory and his decision for NASA to fly AMS as a DOE payload. We also acknowledge the continuous support of the NASA leadership, particularly Ken Bowersox and of the JSC and MSFC flight control teams that have allowed AMS to operate optimally on the ISS for over 14 years. We are grateful for the support of Regina Rameika and Glen Crawford of the DOE including resources from the National Energy Research Scientific Computing Center under Contract No. DE-AC02-05CH11231. We gratefully acknowledge the strong support from CERN including Fabiola Gianotti, and the CERN IT department. We also acknowledge the continuous support from MIT and its School of Science, Nergis Mavalvala, and the Laboratory for Nuclear Science, Boleslaw Wyslouch. Research has been supported by the Chinese Academy of Sciences, Institute of High Energy Physics, National Natural Science Foundation (NSFC), and Ministry of Science and Technology, National Key R&D Program Grants No. 2022YFA1604802 and No. 2022YFA1604803, NSFC Grants No. 12275158 and No. 12305119, the Fundamental Research Funds for the Central Universities, the China Scholarship Council, the provincial governments of Jiangsu, Guangdong, Shandong University, the Shandong Institute of Advanced Technology, and the Sun Yat–sen University Science Foundation, China; Research Council of Finland, Project No. 321882, and Finnish Academy of Sciences and Letters, Grant No. 301123, Finland; CNRS/IN2P3 and CNES, France; DLR under Grants No. 50OO2404, and No. 50OO2501, and computing support on the JARA Partition of the RWTH Aachen supercomputer, Germany; INFN and ASI under ASI-INFN Agreement No. 2019-19-HH.0, its amendments, No. 2021-43-HH.0, and ASI-University of Perugia Agreement No. 2019-2-HH.0, and the Italian Ministry of University and Research (MUR) through the program "*Dipartimenti di Eccellenza 2023-2027*" (Grant SUPER-C), Italy; SECIHTI Grant No. CBF-2025-I-1672 and UNAM Grant DGAPA PAPIIT No. IN111525, Mexico; NWO under Grant No. 680-1-004, Netherlands; FCT under Grant No. 2024.00992.CERN, Portugal; CIEMAT, and IAC CDTI, MCIN-AEI, and under Grants No. PID2022-137810NB-C21/C22, No. PCI2023-145945-2, and No. PCI2023-145961-2 funded by MICIU/AEI/10.13039/501100011033, Spain; the Fondation Dr. Manfred Steuer, Switzerland; Academia Sinica, the National Science and Technology Council (NSTC), formerly the Ministry of Science and Technology (MOST), under Grants No. 114-2123-M-001-007 and No. 114-2112-M-001-029, High Education Sprout Project by the Ministry of Education at National Cheng Kung University, former Presidents of Academia Sinica Yuan-Tseh Lee and Chi-Huey Wong and former Ministers of NSTC (formerly MOST) Maw-Kuen Wu and Luo-Chuan Lee, Taiwan; the Turkish Energy, Nuclear and Mineral Research Agency (TENMAK) under Grant No. 2020TAEK (CERN)A5.H1.F5-26, Türkiye; and NSF Grant No. 2411633 and ANSWERS proposals No. 2149809, No. 2149810, and No. 2149811, LWS NASA Grant/Cooperative Agreement No. 80NSSC20K1819, and FINESST NASA Grant No. 80NSSC21K1392, USA.

Data availability—The data that support the findings of this article are openly available [32]; embargo periods may apply.

[1] I. A. Grenier, J. H. Black, and A. W. Strong, The nine lives of cosmic rays in galaxies, Annu. Rev. Astron. Astrophys. **53**, 199 (2015); P. Blasi, The origin of galactic cosmic rays, Astron. Astrophys. Rev. **21**, 70 (2013); A. W. Strong, I. V. Moskalenko, and V. S. Ptuskin, Cosmic-ray propagation and interactions in the galaxy, Annu. Rev. Nucl. Part. Sci. **57**, 285 (2007); A. Castellina and F. Donato, Diffusion coefficient and acceleration spectrum from direct measurements of charged cosmic ray nuclei, Astropart. Phys. **24**, 146 (2005); G. Jóhannesson *et al.*, Bayesian Analysis of cosmic ray propagation: Evidence against homogeneous diffusion, Astrophys. J. **824**, 16 (2016); M. A. Malkov and L. O'C Drury, Nonlinear theory of diffusive acceleration of particles by shock waves, Rep. Prog. Phys. **64**, 429 (2001).

[2] M. Aguilar *et al.*, Properties of a new group of cosmic nuclei: Results from the Alpha Magnetic Spectrometer on sodium, aluminum, and nitrogen, Phys. Rev. Lett. **127**, 021101 (2021). The measurements of the Na, Al, and N fluxes have been extended to cover same 13.5-year period.

[3] M. Aguilar *et al.*, Properties of neon, magnesium, and silicon primary cosmic rays results from the Alpha Magnetic Spectrometer, Phys. Rev. Lett. **124**, 211102 (2020). The measurements of the Ne, and Mg fluxes have been extended to cover same 13.5-year period.

[4] M. Aguilar *et al.*, Properties of heavy secondary fluorine cosmic rays: Results from the Alpha Magnetic Spectrometer, Phys. Rev. Lett. **126**, 081102 (2021).

[5] M. Aguilar *et al.*, Properties of cosmic-ray sulfur and determination of the composition of primary cosmic-ray carbon, neon, magnesium, and sulfur: Ten-year results from

the Alpha Magnetic Spectrometer, Phys. Rev. Lett. **130**, 211002 (2023).

[6] J. J. Engelmann *et al.*, Charge composition and energy spectra of cosmic-ray nuclei for elements from Be to Ni—Results from HEAO-3-C2, Astron. Astrophys. **233**, 96 (1990).

[7] M. Ave, P. J. Boyle, F. Gahbauer, C. Höppner, J. R. Hörandel, M. Ichimura, D. Müller, and A. Romero-Wolf, Composition of primary cosmic-ray nuclei at high energies, Astrophys. J. **678**, 262 (2008).

[8] J. S. Young, P. S. Freier, C. J. Waddington, N. R. Brewster, and R. K. Fickle, The elemental and isotopic composition of cosmic rays—Silicon to nickel, Astrophys. J. **246**, 1014 (1981).

[9] M. Ichimura *et al.*, Observation of heavy cosmic-ray primaries over the wide energy range from 100 GeV/particle to 100 TeV/particle: Is the celebrated "knee" actually so prominent?, Phys. Rev. D **48**, 1949 (1993).

[10] E. Juliusson, Charge composition and energy spectra of cosmic-ray nuclei at energies above 20 GeV per nucleon, Astrophys. J. **191**, 331 (1974).

[11] J. Lezniak and W. Webber, The charge composition and energy spectra of cosmic-ray nuclei from 3000 MeV per nucleon to 50 GeV per nucleon, Astrophys. J. **223**, 676 (1978).

[12] J. A. Esposito *et al.*, The ALICE instrument and the measured cosmic ray elemental abundances, Astropart. Phys. **1**, 33 (1992).

[13] E. Kamioka *et al.*, Azimuthally controlled observation of heavy cosmic-ray primaries by means of the balloon-borne emulsion chamber, Astropart. Phys. **6**, 155 (1997).

[14] K. Lave *et al.*, Galactic cosmic-ray energy spectra and composition during the 2009–2010 solar minimum period, Astrophys. J. **770**, 117 (2013).

[15] A. Kounine, The Alpha Magnetic Spectrometer on the International Space Station, Int. J. Mod. Phys. E **21**, 1230005 (2012); S. Ting, The Alpha Magnetic Spectrometer on the International Space Station, Nucl. Phys. B, Proc. Suppl. **243–244**, 12 (2013); B. Bertucci, The AMS-02 detector operation in space, Proc. Sci. EPS-HEP2011 (**2011**) 067; M. Incagli, Astroparticle physics with AMS02, AIP Conf. Proc. **1223**, 43 (2010); R. Battiston, The antimatter spectrometer (AMS-02): A particle physics detector in space, Nucl. Instrum. Methods Phys. Res., Sect. A **588**, 227 (2008).

[16] M. Aguilar *et al.*, The Alpha Magnetic Spectrometer (AMS) on the International Space Station: Part II—Results from the first seven years, Phys. Rep. **894**, 1 (2021).

[17] See Supplemental Material at http://link.aps.org/supplemental/10.1103/d2vf-fw3v for the details of the detector description, event selection including backtracing [39] through the geomagnetic field [40], and data analysis. It also contains the tabulated, as functions of rigidity, P, Cl, Ar, K, Ca, Si, F, and S fluxes and P/S, Cl/Ar, and K/Ca flux ratios. In addition, the fitted parameters of Eqs. (2) and (3) are tabulated, as are the AMS C/O, N/O, Ne/Si, Na/Si, Mg/Si, Al/Si, P/Si, S/Si, Cl/Si, Ar/Si, K/Si and Ca/Si abundance ratios at the source together with previous results and the primary and secondary components of C, N, Ne, Na, Mg, and Al fluxes. Figures include the detector layout, the tracker coordinate resolution, the reconstructed event example, the charge selection, the AMS acceptance and efficiency corrections, the Ca break-up probability and Ar and Ca survival probability measurements, the AMS P, Cl, Ar, K, and Ca fluxes as a function of kinetic energy per nucleon together with other measurements, the AMS P/S, Cl/Ar, and K/Ca flux ratios compared with GALPROP-HELMOD, the fit of Eq. (3), and the AMS C, N, Ne, Na, Mg, and Al fluxes, each as the sum of a primary and a secondary component.

[18] J. Alcaraz *et al.*, Leptons in near earth orbit, Phys. Lett. B **484**, 10 (2000).

[19] C. C. Finlay *et al.*, International geomagnetic reference field: The eleventh generation, Geophys. J. Int. **183**, 1216 (2010); E. Thébault *et al.*, Earth Planets Space **67**, 79 (2015); P. Alken, E. Thébault, C. D. Beggan *et al.*, International geomagnetic reference field: The thirteenth generation, Earth Planets Space **73**, 49 (2021).

[20] K. Lübelsmeyer *et al.*, Upgrade of the Alpha Magnetic Spectrometer (AMS-02) for long term operation on the International Space Station (ISS), Nucl. Instrum. Methods Phys. Res., Sect. A **654**, 639 (2011).

[21] B. Alpat *et al.*, The internal alignment and position resolution of the AMS-02 silicon tracker determined with cosmic-ray muons, Nucl. Instrum. Methods Phys. Res., Sect. A **613**, 207 (2010).

[22] Y. Jia, Q. Yan, V. Choutko, H. Liu, and A. Oliva, Nuclei charge measurement by the Alpha Magnetic Spectrometer silicon tracker, Nucl. Instrum. Methods Phys. Res., Sect. A **972** (2020).

[23] G. Ambrosi, V. Choutko, C. Delgado, A. Oliva, Q. Yan, and Y. Li, The spatial resolution of the silicon tracker of the Alpha Magnetic Spectrometer, Nucl. Instrum. Methods Phys. Res., Sect. A **869**, 29 (2017).

[24] Q. Yan and V. Choutko, Alignment of the Alpha Magnetic Spectrometer (AMS) in space, Eur. Phys. J. C **83** (2023).

[25] V. Bindi *et al.*, Calibration and performance of the AMS-02 time of flight detector in space, Nucl. Instrum. Methods Phys. Res., Sect. A **743**, 22 (2014).

[26] M. Aguilar *et al.*, Precision measurement of the helium flux in primary cosmic rays of rigidities 1.9 GV to 3 TV with the Alpha Magnetic Spectrometer on the International Space Station, Phys. Rev. Lett. **115**, 211101 (2015).

[27] J. Allison *et al.*, Recent developments in Geant4, Nucl. Instrum. Methods Phys. Res., Sect. A **835**, 186 (2016); Geant4 developments and applications, IEEE Trans. Nucl. Sci. **53**, 270 (2006); S. Agostinelli *et al.*, Geant4—A simulation toolkit, Nucl. Instrum. Methods Phys. Res., Sect. A **506**, 250 (2003).

[28] Q. Yan, V. Choutko, A. Oliva, and M. Paniccia, Measurements of nuclear interaction cross sections with the Alpha Magnetic Spectrometer on the International Space Station, Nucl. Phys. **A996**, 121712 (2020).

[29] M. Aguilar *et al.*, Precision measurement of the proton flux in primary cosmic rays from rigidity 1 GV to 1.8 TV with the Alpha Magnetic Spectrometer on the International Space Station, Phys. Rev. Lett. **114**, 171103 (2015).

[30] M. Aguilar *et al.*, Properties of iron primary cosmic rays: Results from the Alpha Magnetic Spectrometer, Phys. Rev. Lett. **126**, 041104 (2021). The measurement of the Fe flux has been extended to cover same 13.5-year period.

[31] M. Aguilar *et al.* (AMS Collaboration), Measurement of the heavy nuclei cosmic ray fluxes with the Alpha Magnetic Spectrometer (to be published).

[32] Note that the data can also be downloaded in different formats from the AMS website https://ams02.space/sites/default/files/publication/202601/table-s1.csv, https://ams02.space/sites/default/files/publication/202601/table-s2.csv, https://ams02.space/sites/default/files/publication/202601/table-s3.csv, https://ams02.space/sites/default/files/publication/202601/table-s4.csv, https://ams02.space/sites/default/files/publication/202601/table-s5.csv, https://ams02.space/sites/default/files/publication/202601/table-s6.csv, https://ams02.space/sites/default/files/publication/202601/table-s7.csv, https://ams02.space/sites/default/files/publication/202601/table-s8.csv, https://ams02.space/sites/default/files/publication/202601/table-s9.csv, https://ams02.space/sites/default/files/publication/202601/table-s10.csv, https://ams02.space/sites/default/files/publication/202601/table-s11.csv, the ASI cosmic-ray database at https://tools.ssdc.asi.it/CosmicRays, and the LPSC cosmic-ray database at https://lpsc.in2p3.fr/crdb/.

[33] M. J. Boschini *et al.*, Inference of the local interstellar spectra of cosmic-ray nuclei $Z \leq 28$ with GalProp-HelMod framework, Astrophys. J. Suppl. Ser. **250**, 27 (2020).

[34] M. Aguilar *et al.*, Observation of new properties of secondary cosmic rays lithium, beryllium, and boron by the Alpha Magnetic Spectrometer on the International Space Station, Phys. Rev. Lett. **120**, 021101 (2018). The measurements of the Li, Be, and B fluxes have been extended to cover same 13.5-year period.

[35] G. D. Lafferty and T. R. Wyatt, Where to stick your data points: The treatment of measurements within wide bins, Nucl. Instrum. Methods Phys. Res., Sect. A **355**, 541 (1995). We have used Eq. (6) with $\tilde{R} \equiv x_{lw}$.

[36] M. A. DuVernois and M. R. Thayer, The elemental composition of the galactic cosmic-ray source: Ulysses high-energy telescope results, Astrophys. J. **465**, 982 (1996).

[37] A. C. Cummings, E. C. Stone, B. C. Heikkila, N. Lal, W. R. Webber, G. Jóhannesson, I. V. Moskalenko, E. Orlando, and T. A. Porter, Galactic cosmic rays in the local interstellar medium: Voyager 1 observations and model results, Astrophys. J. **831**, 18 (2016).

[38] M. H. Israel *et al.*, Elemental composition at the cosmic-ray source derived from the ACE-CRIS instrument. I. $_6$C to $_{28}$Ni, Astrophys. J. **865**, 69 (2018).

[39] A. C. Cummings, I. V. Moskalenko, B. C. Heikkila, G. Jóhannesson, and T. A. Porter, Voyager 1 observations of galactic cosmic-ray isotopes in the very local interstellar medium: Evidence for primary ^{2}H and B, Astrophys. J. **993**, 81 (2025).

[40] M. Aguilar *et al.*, Observation of the identical rigidity dependence of He, C, and O cosmic rays at high rigidities by the Alpha Magnetic Spectrometer on the International Space Station, Phys. Rev. Lett. **119**, 251101 (2017). The measurements of the He, C, and O fluxes have been extended to cover same 13.5-year period.